Instruction-driven history-aware policies for robotic manipulations

Pierre-Louis Guhur[1], **Shizhe Chen**[1], **Ricardo Garcia**[1],
Makarand Tapaswi[2], **Ivan Laptev**[1], **Cordelia Schmid**[1]
[1]Inria, École normale supérieure, CNRS, PSL Research University [2]IIIT Hyderabad
https://guhur.github.io/hiveformer/

Abstract: In human environments, robots are expected to accomplish a variety of manipulation tasks given simple natural language instructions. Yet, robotic manipulation is extremely challenging as it requires fine-grained motor control, long-term memory as well as generalization to previously unseen tasks and environments. To address these challenges, we propose a unified transformer-based approach that takes into account multiple inputs. In particular, our transformer architecture integrates (i) natural language instructions and (ii) multi-view scene observations while (iii) keeping track of the full history of observations and actions. Such an approach enables learning dependencies between history and instructions and improves manipulation precision using multiple views. We evaluate our method on the challenging RLBench benchmark and on a real-world robot. Notably, our approach scales to 74 diverse RLBench tasks and outperforms the state of the art. We also address instruction-conditioned tasks and demonstrate excellent generalization to previously unseen variations.

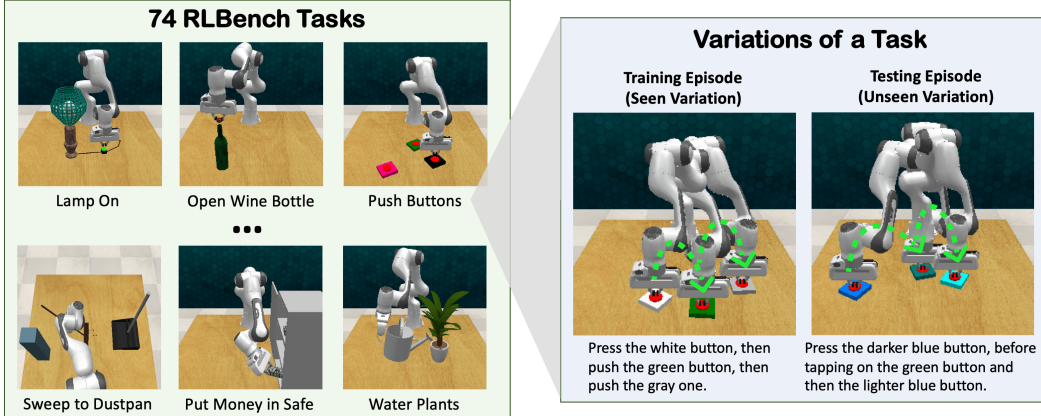**Keywords:** Robotics Manipulation, Language Instruction, Transformer

1 Introduction

People can naturally follow language instructions and manipulate objects to accomplish a wide range of tasks from cooking to assembly and repair. It is also easy to generalize to new tasks by building upon skills learned from previously seen tasks. Hence, one of the long-term goals for robotics is to create generic instruction-following agents that can generalize to multiple tasks and environments.

Thanks to significant advances in learning generic representations for vision and language [2, 3, 4, 5], recent work has made great progress towards this goal [6, 7, 8, 9, 10]. For example, CLIPort [9] exploits CLIP models [5] to encode single-step visual observations and language instructions and to learn a single policy for 10 simulated tasks. BC-Z [10] uses a pre-trained sentence encoder [11] to generalize to multiple manipulation tasks. However, several challenges remain underexplored. One important challenge is that sequential tasks require to track object states that may be hidden from current observations, or to remember previously executed actions. This behaviour is hard to model with recent methods that mainly rely on current observations [9, 10].

Another challenge concerns manipulation tasks that require precise control of the robot end-effector to reach target locations. Such tasks can be difficult to solve with single-view approaches [12], especially in situations with visual occlusions and objects of different sizes, *e.g.* see *put money in safe* Figure 1 (left). While several recent approaches combine views from multiple cameras by converting multi-view images into a unified 2D/3D space [13, 14] or through a late fusion of multi-view predictions [15], learning representations for multiple camera views is an open research problem. Furthermore, cross-modal alignment between vision, action, and text is challenging, in particular when training and test tasks differ in terms of objects and the order of actions, see Figure 1 (right). Most of existing methods [9, 10, 16, 17] condense instructions into a global vector to condition policies [18] and are prone to lose fine-grained information about different objects.

To address the above challenges, we introduce *Hiveformer* - a **H**istory-aware **i**nstruction-conditioned multi-**vi**ew trans**former**. It converts instructions into language tokens given a pre-trained language encoder [5], and combines visual tokens for both past and current visual observations and proprioception. These tokens are concatenated and fed into a multimodal transformer which jointly models dependencies between the current and past observations, spatial relations among views from multi-

Figure 1: Left: Hiveformer can adapt to perform 74 tasks from RLBench [19] given language instructions. **Right:** Multiple variations of the *push buttons* task.

ple cameras, as well as fine-grained cross-modal alignment between vision and instruction. Based on the output representations from our multimodal transformer, we predict 7-DoF actions, *i.e.*, position, rotation and state of the gripper, with a UNet [20] decoder.

We carry out extensive experiments on RLBench [19] in three setups: single-task learning, multi-task learning, and multi-variation generalization[1]. Our Hiveformer significantly outperforms state-of-the-art models for all three settings, demonstrating the effectiveness of encoding instruction, history and views from multiple cameras with the proposed transformer. Moreover, we evaluate our model on 74 tasks of RLBench, which goes beyond the 10 tasks used by Liu *et al.* [15]. We manually group all the tasks into 9 categories according to their main challenges and analyze results per category for a better understanding. Hiveformer not only excels in the multiple task setting with seen instructions in training, but also enables generalization to new instructions that represent different variations of the task, even with human-written language instructions. Finally, we evaluate our model deployed on a real robot and show excellent performance. Interestingly, pretraining the model in the RLBench simulator results in significant performance gains when only a small number of real robot demonstrations are available.

To summarize, our contributions are three-fold:

- We introduce a new model, Hiveformer, to solve various challenges in robotics tasks. It jointly models an instruction, multiple views, and history via a multimodal transformer for action prediction in robotic manipulation.
- We perform extensive ablations of our model on RLBench with 74 tasks grouped into 9 distinct categories. The history improves long-term tasks and the multi-view setting is most helpful for tasks requiring high precision or in the presence of visual occlusions.
- We demonstrate that Hiveformer outperforms the state of the art in three RLBench setups, namely single-task, multi-task and multi-variation. A single Hiveformer trained with synthetic instructions is able to solve multiple tasks and task variations, can generalize to unseen human-written instructions and shows excellent performance on a real robot after finetuning.

Our code, pre-trained models and additional results are available on the project webpage [1].

2 Related Work

Vision-based robotic manipulation. While earlier methods for solving robotics tasks such as visual servoing [21, 22] were designed manually, the need to cope with large variations of objects and environments led to the emergence of learning-based neural approaches [23, 24, 25, 26]. Deep neural networks [27, 28] have achieved impressive results in manipulation for single tasks [29], and recently led to more challenging setups such as multi-task learning [30, 31, 32, 33]. Different multi-task approaches are explored by discovering which tasks should be trained together [15, 34], determining

---

[1]We follow definitions in RLBench [19] for tasks and variations. A task can be composed of multiple variations that share the same skills but differ in objects, attributes or order as shown in Figure 1 (right).

shared features across tasks [35, 36], meta-learning [37, 38, 39], goal-conditioned learning [40, 41], or inverse reinforcement learning [42]. These approaches can be generally split in two categories according to the training algorithm: reinforcement learning (RL) methods [43, 44, 45, 46] which learn policies from rewards provided by environments and behavioral cloning methods [47, 48, 49] that learn from demonstrations using supervised learning. Demonstrations can be obtained from humans [50], robots [23, 51] or play interactions [49]. The emergence of robotic simulators, such as Gym [52], manipulaTHOR [53], dm_control [54], Sapien [55], CausalWorld [56], and RL-Bench [19], also greatly accelerated the development of manipulation methods. In this work, we use behavioral cloning to train policies given scripted demonstrations from RLBench [19] which covers many challenging manipulation tasks.

Instruction-driven vision-based robotic manipulation has received growing attention for manipulations in 2D planar [57, 58] or recent 3D environments [8, 59, 60], and has been transferred to the real world [9, 10]. As grounding the language in visual scenes is important, existing works have focused on challenges in object grounding, such as localizing objects based on referring expressions [61, 62, 63] and grounding spatial relationships [7, 64, 65]. Since language describes high-level actions, several works [60, 66, 67] consider a hierarchical approach to decompose a task into sub-goals. Because natural language is rich and diverse, while training resources are limited, further works learn from collected offline data with instructions [10, 17] or leverage pre-trained vision-language models [4, 5] for action prediction [9, 68]. To further improve the precision of manipulation skills, Mees *et al.* [8] align instructions with multiple cameras by fusing input images with known camera parameters. Most of these works [6, 8, 9, 10] are stateless, since they only employ current observations to predict next actions. Instead, our work proposes to jointly model language instructions, history, and multi-view observations.
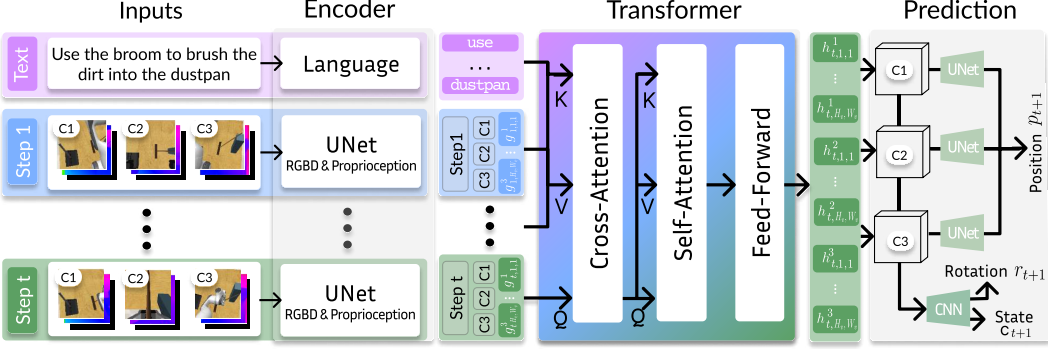
Transformers [69] have led to significant gains in natural language processing [2], computer vision [70] and related fields [4, 5, 71]. They have also been used in the context of supervised reinforcement learning, such as Decision Transformer [72] or Trajectory Transformer [73]. Recent works in Vision-and-Language Navigation (VLN) [74, 75, 76] further demonstrate that the Transformer allows to better leverage previous observations to improve multi-modal action prediction. Transformers are also used to build a multi-modal, multi-task, multi-embodiment generalist agent, GATO [77]. Inspired by the success of transformers, we explore the transformer architecture for instruction-driven and history-aware robotic manipulation.

3 Problem Definition

Our goal is to train a policy $\pi\left(a_{t+1}|\{x_l\}_{l=1}^n, \{o_i\}_{i=1}^t, \{a_i\}_{i=1}^t\right)$ for robotic manipulation conditioned on a natural language instruction $\{x_l\}_{l=1}^n$, visual observations $\{o_i\}_{i=1}^t$, and previous actions $\{a_i\}_{i=1}^t$ where n is the number of words in the instruction and t is the current step. For robotic control, we use macro steps [12] – key turning points in action trajectories where the gripper changes its state (open/close) or velocities of joints are close to zero. We employ an inverse-kinematics based controller to find a trajectory between macro-steps. In this way, the sequence length of an episode is significantly reduced from hundreds of small steps to typically less than 10 macro steps.

The **observation** o_t at step t consists of RGB images I_t and point clouds P_t aligned with the RGB images. I_t is composed of $\{I_t^k\}_{k=1}^K$ RGB images from K cameras, with each I_t^k being of size $H \times W \times 3$ (height, width, 3 channels). Following [15], we use $K = 3$ with cameras on the wrist, left shoulder and right shoulder of the agent, and $H = W = 128$. Similarly, P_t represents point clouds $\{P_t^k\}_{k=1}^K$ from $K = 3$ cameras. A point cloud $P_t^k \in \mathbb{R}^{H \times W \times 3}$ is obtained by projecting a single channel depth image $H \times W$ from the k-th camera in world coordinates using known camera intrinsics and extrinsics. Each point in P_t^k has thus 3D coordinates and is aligned with a pixel in I_t^k.

The **action space** a_t consists of the gripper pose and its state following the standard setup in RL-Bench [12]. The gripper pose is composed of the Cartesian coordinates $p_t = (x_t, y_t, z_t)$ and its rotation described by a quaternion $q_t = (q_t^0, q_t^1, q_t^2, q_t^3)$ relative to the base frame. The gripper's state c_t is boolean and indicates whether the gripper is open or closed. An object is grasped when it is located in between the gripper's two fingers and the gripper is closing its grasp. The execution of an action is achieved by a motion planner in RLBench.

Figure 2: Hiveformer jointly models instructions, views from multiple cameras, and past actions and observations with a multimodal transformer for robotic manipulation.

4 Our Model: Hiveformer

We propose a unified architecture for robotic tasks called Hiveformer (**Hi**story-aware **i**nstruction-conditioned multi-**vi**ew trans**former**), see Figure 2 for an overview. It consists of three modules: feature encoding, multimodal transformer and action prediction. The feature encoding module (Sec. 4.1) generates token embeddings for instructions $\{x_l\}_{l=1}^n$, visual observations $\{o_i\}_{i=1}^t$ and previous actions $\{a_i\}_{i=1}^t$. Then, the multimodal transformer (Sec. 4.2) learns relationships between the instruction, current multi-camera observations and history. Finally, the action prediction module (Sec. 4.3) utilizes a convolutional network (CNN) to predict the next rotation q_{t+1} and gripper state c_{t+1}, and adopts a UNet decoder [20] to predict the next position p_{t+1}.

4.1 Feature Encoding

We encode the instruction, visual observations, and actions as a sequence of tokens.

Instructions. We employ a pre-trained language encoder to tokenize and encode the sentence instruction. Specifically, we use the language encoder in the CLIP model [5]. Thanks to its vision-and-language pre-training, it is better at differentiating vision-related semantics such as colors compared to pure language-only pre-trained models like BERT [2], see Table 7 in the appendix. We freeze the pre-trained language encoder and use a linear layer on top of it to obtain embeddings $\hat{x}_l \in \mathbb{R}^d$ for each word token:

$$\hat{x}_l = \text{LN}(W_x \tilde{x}_l) + E_T^x, \tag{1}$$

with $\tilde{x}_l$ the l-th embedding output by the language encoder, LN layer normalization [78], W_x a projection matrix, and E_T^x a type embedding which differentiates instructions from visual observations.

Observations and Proprioception. We encode the RGB image I_t^k, point clouds P_t^k, and proprioception A_t^k for each camera k separately. $A_t^k \in \{0,1\}^{H \times W}$ is a binary attention map used to encode the position of the gripper p_t. It takes value one at the location of the gripper center and zero elsewhere. We concatenate I_t^k and A_t^k in the channel dimension and use a UNet encoder to obtain a feature map $\hat{F}_t^k \in \mathbb{R}^{H^v \times W^v \times d_v}$, where H^v, W^v, d_v are the height, width, and number of channels of the feature map. More details about the CNN architecture are presented in Section A of the appendix. Next, we concatenate $\hat{F}_t^k$ with point cloud representations in the channel dimension to indicate the spatial location of each patch in the feature map. To match the size of P_t^k and $\hat{F}_t^k$, we apply mean-pooling to P_t^k. The final encoded feature map $F_t^k \in \mathbb{R}^{H^v \times W^v \times (d_v+3)}$ is computed as follows:

$$F_t^k = \left[\text{CNN}([I_t^k; A_t^k]); \text{MeanPool}(P_t^k)\right]. \tag{2}$$

We use patches $f_{t,h,w}^k \in F_t^k, h \in [1, H^v], w \in [1, W^v]$ as separate visual tokens. We further encode $f_{t,h,w}^k$ using embeddings of the camera id E_C^k, of the step id E_S^t, and of the patch location $E_L^{h,w}$ as well as an embedding to indicate the visual nature of the tokens E_T^v as follows:

$$g_{t,h,w}^k = \text{LN}(W_f f_{t,h,w}^k) + E_C^k + E_S^t + E_L^{h,w} + E_T^v. \tag{3}$$

The encoded visual tokens of the k-th camera at step t are denoted as $G_t^k = \{g_{t,h,w}^k\}_{h=1,w=1}^{H^v,W^v} \in \mathbb{R}^{H^v \times W^v \times d}$. We concatenate the encoded tokens for all cameras as $G_t = (G_t^1, \cdots, G_t^K)$.

4

4.2 Multimodal transformer

Given the encoded tokens at the current macro step t, the multimodal transformer aims to obtain a contextualized representation for G_t conditioned on the encoded instruction $\{\hat{x}_l\}_{l=1}^{n}$ and history $\{G_i\}_{i=1}^{t-1}$. This enables learning relationships among views from multiple cameras, the current observations and instructions, and between the current observations and history for action prediction. We use the transformer's attention mechanism [79] to learn such relationships:

$$\text{Attn}(Q,K,V) = \text{Softmax}\left(\frac{W_Q Q (W_K K)^T}{\sqrt{d}}\right) W_V V, \tag{4}$$

where W_Q, W_K, W_V are learnable parameters. Unlike previous work [75] that uses self-attention layers to capture all relationships, we employ different attention layers to capture different types of relationships, in order to reinforce the importance of the context. First, we use a cross-attention layer to learn the inter-modal relationships between G_t and its conditioned contexts C_t consisting of tokens in the instruction $\{\hat{x}_l\}_{l=1}^{n}$ and history $\{G_i\}_{i=1}^{t-1}$, which is:

$$\tilde{G}_t = \text{CA}(G_t, C_t) = \text{Attn}\left(G_t, C_t, C_t\right). \tag{5}$$

Then we learn the intra-modal relationships among patch tokens obtained from the views from multiple cameras through a self-attention layer, *i.e.* $\text{SA}(\tilde{G}_t) = \text{Attn}(\tilde{G}_t, \tilde{G}_t, \tilde{G}_t)$. Finally, a feed-forward network consisting of two linear layers W_1 and W_2 is applied as follows:

$$\hat{G}_t = \text{LN}\left(W_2 \,\text{GeLU}\left(W_1 \,\text{SA}(\tilde{G}_t)\right)\right). \tag{6}$$

4.3 Action Prediction

We concatenate the output embeddings of the transformer $\hat{G}_t$ in Eq (6) and the original encoded visual representations $\hat{F}_t$ in Sec. 4.1 in the channel dimension and reshape the flattened sequence into a feature map $H_t \in \mathbb{R}^{K \times H^v \times W^v \times (d+d_v)}$ to predict the next action $a_{t+1} = [p_{t+1}; q_{t+1}; c_{t+1}]$. As some RLBench tasks require accurate fine-grained positioning, different from the rotation q_{t+1} and gripper state c_{t+1}, the position p_{t+1} is predicted through a separate module that uses point clouds P_t.

Rotation and gripper's state. We transform H_t into $\mathbb{R}^{H^v \times W^v \times K(d+d_v)}$ and feed it into a CNN decoder, described in Section A of the appendix. We then apply average pooling across spatial dimensions and employ a linear layer to regress a 5-dimension vector $[q_{t+1}; c_{t+1}]$.

Position. The prediction of the gripper position p_{t+1} is decomposed into an expected point on point clouds p_{t+1}^e and an offset p_{t+1}^o, *i.e.* $p_{t+1} = p_{t+1}^e + p_{t+1}^o$. The offset allows us to predict a virtual point outside the convex hull of the point cloud, *e.g.* when a robotic arm reaches first above the object and then touch the object. For each camera k, a CNN with an upsampling layer predicts an attention map $B_t^k \in \mathbb{R}^{H \times W}$ over the point clouds P_t^k. Each value $B_{t,h,w}^k \in B_t^k$ corresponds to the probability of reaching the point $P_{t,h,w}^k \in P_t^k$. Therefore, we compute p_{t+1}^e as the expected position over all cameras:

$$p_{t+1}^e = \sum_{k,h,w} \left(B_{t,h,w}^k \cdot P_{t,h,w}^k\right). \tag{7}$$

The offset p_{t+1}^o is computed from the instruction and the current step id. Let $E_O \in \mathbb{R}^{N_\tau \times T \times 3}$ be a learnable embedding, where N_τ is the number of tasks and T is the maximum length of episodes. We predict the task id from the instruction: $\Pr(m) = \text{Softmax}\left(W_m \frac{1}{n}\sum_{l=1}^{n}\tilde{x}_l\right)$, where $\Pr(m) \in [0,1]^{N_\tau}$, and we obtain the offset as: $p_{t+1}^o = \sum_m \Pr(m) \cdot E_O(m,t,:)$.

4.4 Training and Inference

Losses. We use behavioral cloning to train the models. In RLBench, we generate D, a collection of N successful demonstrations for each task. Each demonstration $\delta \in$ D is composed of a sequence of (maximum) T macro-steps with observations $\{o_i^\delta\}_{i=1}^{T}$, actions $\{a_i^*\}_{i=1}^{T}$, task m^* and instruction $\{x_l\}_{l=1}^{n}$. We minimize a loss function $\mathscr{L}$ over a batch of demonstrations $\text{B} = \{\delta_j\}_{j=1}^{|B|} \subset$ D. The loss function is the sum of two losses: a mean-square error (MSE) on the gripper's action and a cross-entropy (CE) over the task classification:

$$\mathscr{L} = \frac{1}{|B|} \sum_{\delta \in \text{B}} \left[\sum_{t \leq T} \text{MSE}\left(a_t, a_t^*\right) + \text{CE}\left(\Pr(m), m^*\right)\right]. \tag{8}$$

5

Table 1: Success rate on the single-task setting. We report mean and variance for unseen episodes.

	Inputs			Transformer			Training	SR
	Visual Tokens	Point Clouds	Gripper Position	Multi-View	History	Attn	Mask Obs	
R1	$\times$	$\times$	$\times$	$\times$	$\times$	$\times$	$\times$	72.9 ± 4.1
R2	Channel	$\times$	$\times$	$\checkmark$	$\times$	Self	$\times$	73.1 ± 4.5
R3	Channel	$\checkmark$	$\times$	$\checkmark$	$\times$	Self	$\times$	77.1 ± 5.8
R4	Channel	$\checkmark$	$\checkmark$	$\checkmark$	$\times$	Self	$\times$	78.1 ± 5.8
R5	Channel	$\checkmark$	$\checkmark$	$\checkmark$	$\checkmark$	Self	$\times$	81.8 ± 5.2
R6	Channel	$\checkmark$	$\checkmark$	$\checkmark$	$\checkmark$	Self	$\checkmark$	82.3 ± 5.3
R7	Patch	$\checkmark$	$\checkmark$	$\checkmark$	$\checkmark$	Self	$\checkmark$	84.4 ± 6.4
R8	Patch	$\checkmark$	$\checkmark$	$\checkmark$	$\checkmark$	Cross	$\checkmark$	88.4 ± 4.9

Masking current observation. To ensure that the model uses past information $\{o_i\}_{i=1}^{t-1}, \{a_i\}_{i=1}^{t-1}$ instead of only relying on the current observation o_t, we randomly mask the current observation with a probability of 0.1. The masking zeros out randomly selected patch features in the current observation. Therefore, even if the unmasked current observations contain sufficient information, the model still requires to complete the masked observations from the history for action prediction.

5 Experiments

In this section we present experiments on RLBench [19] tasks to demonstrate the effectiveness of our Hiveformer model in three settings: single-task, multi-task, and multi-variation. In the single-task setup, a separate model is trained and tested for each task with no variations of the task. Multi-task refers to a setting where one model is trained for multiple tasks (but each task has a unique variation). In the multi-variation case we train a single model to solve multiple variations of a single task and test it on new variations of the task unseen during training.

5.1 Experimental Setup

Dataset setups. RLBench [19] is a benchmark of robotic tasks. To compare our method with previous work [15], we use the same 10 tasks with 100 demonstrations for training unless stated otherwise. We further evaluate our model on 74 tasks for which RLBench provides successful demonstrations. We manually group these tasks into 9 categories according to their challenges. More details on the split of the tasks are given in Section B of the Appendix. We evaluate models by measuring the per task success rate for 500 unseen episodes.

Implementation details. We use the Adam optimizer with a learning rate of 5×10^{-5}. Each batch consists of 32 demonstrations. Models were trained for 100,000 iterations. We apply data augmentation in training including jitter over RGB images I_t^k, and a random crop of I_t^k, P_t^k, and A_t^k while keeping them aligned. Models are trained on one NVIDIA Tesla V100 SXM2 GPU using a Singularity container with headless rendering. Auto-λ [15] uses a UNet network and applies late fusion to predictions from multiple views.

5.2 Ablations

To demonstrate the effectiveness of the proposed model architecture, we ablate the impact of its components in Table 1. The model in R1 (row 1) is a UNet architecture similar to Auto-λ [15] except that it is conditioned on instructions rather than task ids. This baseline only uses visual observations at the current step and already achieves promising results with a success rate of 73.2%. On top of R1's architecture, a multimodal transformer with self-attention is added in R2 to improve the modeling of multi-view images. Visual tokens $\{G_t^i\}_{i=1}^K$ are different channels in the feature map instead of spatial patches used in our final model. In R3 and R4, we further add point clouds P_t and gripper position A_t in the feature encoding, which leads to 3% improvement in total. The impact of history, *i.e.* the use of observations from previous steps, $(\{G_j^i\}_{i=1,j=1}^{K,t-1})$ is studied in R5 and R6. The history information brings 4.5% absolute gains and the masking of observations during training further improves the performance by 0.5%. In R7, we replace the tokenization of feature maps from channels $g_{t,c}^k$ to patches $g_{t,h,w}^k$, and obtain another 2.2% gain. This improvement can be attributed

Table 2: Comparison with state-of-the-art methods on 10 tasks. We report success rate (%).

	Pick & Lift	Pick-Up Cup	Push Button	Put Knife	Put Money	Reach Target	Slide Block	Stack Wine	Take Money	Take Umbrella	Avg.
Single-task learning											
ARM [12]	70	80	-	-	-	100	-	70	-	70	-
Auto-λ [15]	82	72	95	36	31	100	36	23	38	37	55.0
Ours	92.2	77.1	99.6	69.7	96.2	100.0	95.4	81.9	82.1	90.1	88.4
Multi-task learning											
Auto-λ [15]	87	78	95	31	62	100	77	19	64	80	69.3
Ours (w/o inst)	83.8	13.9	97.0	41.9	54.3	98.9	36.2	68.5	74.1	73.0	64.2
Ours	88.9	92.9	100.0	75.3	58.2	100.0	78.7	71.2	79.1	89.2	83.3

Table 3: Comparison with the state of the art on 74 RLBench tasks grouped into 9 categories. We report success rate (%) for the single-task setting. *The performance of Auto-λ is obtained by running their code.

	Planning	Tools	Long Term	Rot. Invar.	Motion Planning	Screw	Multi Modal	Precision	Visual Occlusion	Avg
Num. of tasks	9	11	4	7	9	4	5	11	14	74
Auto-λ [15]*	58.9	20.0	2.3	73.1	66.7	48.2	47.6	34.6	40.6	44.0
Ours (w/o hist)	78.9	46.7	10.0	84.6	73.3	72.6	60.0	63.8	57.9	60.9
Ours (one view)	57.7	23.2	12.3	57.8	63.2	35.6	40.7	33.7	37.1	40.1
Ours	81.6	53.0	16.9	84.2	72.7	80.9	67.1	64.7	60.2	65.4

to patch tokens that help encode fine-grained spatial information. Finally, we use cross-attention instead of self-attention (Eq. 5) to condition on the instruction and history context. It further boosts the performance with a 3.8% gain.

5.3 Comparison with State of the Art

Single-task evaluation. The upper block in Table 2 presents results of different models on 10 single tasks in RLBench. We compare our model with ARM [12] and Auto-λ [15], two state-of-the-art methods on RLBench and observe a consistent improvement for all tasks.

Extending tasks in a single-task evaluation setup. In Table 3, we further compare Auto-λ and Hiveformer's variants across 74 RLBench tasks grouped into 9 categories. The variant without history removes the history tokens in Hiveformer, while the variant with one view only uses one camera at each step (we take the best among the 3 cameras for each task). The full Hiveformer achieves consistently better performance compared to Auto-λ [15] on all types of tasks. Among them, the Long-term, Tools and Planning task groups assess the use of history, where our model brings improves significantly over the variant without history. Compared to the one view variant, our full model performs significantly better on tasks requiring fine-grained control or with large occlusions such as Screw, Precision and Visual Occlusion categories. Yet, our method performs relatively poorly for Long-term tasks with more than 10 steps, such as "take shoes out of box". As Long-term tasks have an average number of steps 2-4 times higher than others, they are more prone to distribution shift issues and accumulated errors. Hierarchical modeling or better training algorithms such as reinforcement learning and dagger [80] could be helpful, but are left as future work.

Multi-task evaluation. The lower half in Table 2 shows the results in a multi-task setting. Notably, Auto-λ uses a training algorithm which dynamically adjusts the weights of different tasks, while our model simply treats all tasks with equal weights. Nevertheless, our model outperforms Auto-λ by 14%, demonstrating the improvements due to our architecture. We further compare our model with a variant without instructions in the input sequence (since p_{t+1}^o is predicted from instructions, we modify the model such as it is predicted from H_t^k). The results show that instructions are important in the multi-task setting.

Moreover, the performance of our *single* model trained for all tasks is only slightly worse than the performance of individual models for each task.

Table 4: Success rate (%) in the multi-variation setting for seen or unseen variations and synthetic or human-written instructions.

# Demos Per Variation	Push Buttons			Tower		
	Seen var.	Unseen var.		Seen	Unseen var.	
	Synthetic	Synthetic	Human	Synthetic	Synthetic	Human
10	96.8	73.1	65.1	71.7	50.1	19.4
50	99.6	83.3	70.6	74.1	52.3	20.7
100	100	86.4	74.0	76.2	56.4	24.2

Generalization to multi-variations. Table 4 shows results of Hiveformer trained on different variations of the two tasks *Tower* and *Push Buttons*. The *Tower* (resp. *Push Buttons*) task requires the robot to sequentially stack colored cubes (resp. push colored buttons) using the order specified in the instruction, see Figure 1 (right). We use 100 variations in training and test models for both the 100 seen variations and 100 unseen variations. In this setting, instructions are necessary to generalize to unseen variations (*e.g.* it is impossible to distinguish the order of pushing buttons red-green-blue vs. blue-red-green by only looking at the scene). We compare the models trained with different numbers of demonstrations per variation. Even in the most challenging case where only 10 demonstrations are available per variation, Hiveformer achieves a success rate of 71.1% for the *push buttons* task and 49.8% for the *tower* task in unseen variations. Furthermore, besides tests on synthetic instructions (Synt), we also test the generalization to real instructions. Despite being only trained on synthetic instructions with limited vocabulary and diversity, our model performs well on instructions generated by humans (Real). Finetuning Hiveformer on human instructions [75] is expected to result in further improvements. Details of human-generated instructions are presented in Section C of the Appendix.

5.4 Real-robot Experiments

Setup. We conduct real-robot experiments for the *push buttons* task on a 6-DoF UR5 robotic arm equipped with a 2-finger Robotiq RG2 gripper and two cameras on each side of the scene. As there exists a large difference between simulated and real environments, we finetune the simulator-trained policy on real-robot demonstrations. We use 10 variations of the task and 10 real-robot demonstrations per variation. More details are presented in Section E of the Appendix.

Results. We report success rates for real-robot experiments in Table 5 on the "push buttons" task using synthetic instructions. The models are tested on 10 seen and 10 unseen variations. We compare two models: one trained from scratch using real-robot demonstrations; and the other pretrained on RLBench and then finetuned using real-robot demonstrations. As shown in Table 5, the pretraining significantly improves the performance especially for unseen variations. The model without pretraining is prone to overfitting on seen variations. Although the domain gap between the real robot and RLBench environments is large, our model benefits from pretraining in the simulator. More analysis and examples are presented in Section E of the Appendix.

Table 5: Success rate of push buttons task on real robots.

Pretrain	Seen Vars	Unseen Vars
-	86.7	13.3
✓	92.2	85.7

6 Conclusion

We introduced Hiveformer, a multimodal transformer that jointly models instructions, views from multiple cameras, and history for instruction-driven robotics manipulation. We evaluated the model on RLBench in three settings: single-task learning, multi-task learning, and multi-variation generalization and demonstrated its effectiveness outperforming state-of-the-art. We deployed our model on a real robot which is able to generalize to unseen variations and human-written instructions.

Limitations. The computational cost quadratically increases with the input sequence length due to the transformer. Furthermore, our model is trained with behavioral cloning, which may suffer from exposure bias. Future works could improve the efficiency for long-term tasks with hierarchical models and also incorporate reinforcement learning. Moreover, our model is trained on only synthetic instructions and performs worse on the human-written instructions. Training on human-written automatically generated instructions could help improve the performance.

References

[1] Project webpage. https://guhur.github.io/hiveformer/.

[2] J. Devlin, M.-W. Chang, K. Lee, and K. Toutanova. BERT: Pre-training of deep bidirectional transformers for language understanding. In *NAACL-HLT*, 2019.

[3] K. He, H. Fan, Y. Wu, S. Xie, and R. Girshick. Momentum contrast for unsupervised visual representation learning. In *CVPR*, 2020.

[4] J. Lu, D. Batra, D. Parikh, and S. Lee. ViLBERT: Pretraining task-agnostic visiolinguistic representations for vision-and-language tasks. In *NeurIPS*, 2019.

[5] A. Radford, J. W. Kim, C. Hallacy, A. Ramesh, G. Goh, S. Agarwal, G. Sastry, A. Askell, P. Mishkin, J. Clark, et al. Learning transferable visual models from natural language supervision. In *ICML*, pages 8748–8763. PMLR, 2021.

[6] C. Lynch and P. Sermanet. Language conditioned imitation learning over unstructured data. *RSS*, 2021.

[7] O. Mees and W. Burgard. Composing pick-and-place tasks by grounding language. In *ISER*, 2021.

[8] O. Mees, L. Hermann, E. Rosete-Beas, and W. Burgard. CALVIN: A benchmark for language-conditioned policy learning for long-horizon robot manipulation tasks. *RA-L*, 2022.

[9] M. Shridhar, L. Manuelli, and D. Fox. CLIPort: What and where pathways for robotic manipulation. In *CoRL*, pages 894–906. PMLR, 2022.

[10] E. Jang, A. Irpan, M. Khansari, D. Kappler, F. Ebert, C. Lynch, S. Levine, and C. Finn. BC-Z: Zero-shot task generalization with robotic imitation learning. In *CoRL*, pages 991–1002. PMLR, 2022.

[11] Y. Yang, D. Cer, A. Ahmad, M. Guo, J. Law, N. Constant, G. H. Abrego, S. Yuan, C. Tar, Y.-H. Sung, et al. Multilingual universal sentence encoder for semantic retrieval. In *ACL*, pages 87–94, 2020.

[12] S. James and A. J. Davison. Q-Attention: Enabling efficient learning for vision-based robotic manipulation. *RA-L*, 2022.

[13] A. Zeng, P. Florence, J. Tompson, S. Welker, J. Chien, M. Attarian, T. Armstrong, I. Krasin, D. Duong, V. Sindhwani, et al. Transporter networks: Rearranging the visual world for robotic manipulation. In *CoRL*, pages 726–747. PMLR, 2021.

[14] S. James, K. Wada, T. Laidlow, and A. J. Davison. Coarse-to-fine Q-Attention: Efficient learning for visual robotic manipulation via discretisation. In *CVPR*, 2022.

[15] S. Liu, S. James, A. J. Davison, and E. Johns. Auto-Lambda: Disentangling dynamic task relationships. *TMLR*, 2022.

[16] L. Shao, T. Migimatsu, Q. Zhang, K. Yang, and J. Bohg. Concept2robot: Learning manipulation concepts from instructions and human demonstrations. *The International Journal of Robotics Research*, 40(12-14):1419–1434, 2021.

[17] S. Nair, E. Mitchell, K. Chen, S. Savarese, C. Finn, et al. Learning language-conditioned robot behavior from offline data and crowd-sourced annotation. In *CoRL*, pages 1303–1315. PMLR, 2022.

[18] E. Perez, F. Strub, H. De Vries, V. Dumoulin, and A. Courville. FiLM: Visual reasoning with a general conditioning layer. In *AAAI*, 2018.

[19] S. James, Z. Ma, D. R. Arrojo, and A. J. Davison. RLBench: The robot learning benchmark & learning environment. *RA-L*, 5(2):3019–3026, 2020.

[20] O. Ronneberger, P. Fischer, and T. Brox. UNet: Convolutional networks for biomedical image segmentation. In *International Conference on Medical image computing and computer-assisted intervention*, pages 234–241. Springer, 2015.

[21] J. Hill. Real time control of a robot with a mobile camera. In *9th Int. Symp. on Industrial Robots, 1979*, pages 233–246, 1979.

[22] F. Chaumette and S. Hutchinson. Visual servo control. i. basic approaches. *IEEE Robotics & Automation Magazine*, 13(4):82–90, 2006.

[23] R. Strudel, A. Pashevich, I. Kalevatykh, I. Laptev, and C. Schmid. Learning to combine primitive skills: A step towards versatile robotic manipulation. In *ICRA*, pages 4637–4643. IEEE, 2020.

[24] A. X. Lee, S. Levine, and P. Abbeel. Learning visual servoing with deep features and fitted q-iteration. In *ICLR*, 2017.

[25] Q. Bateux, E. Marchand, J. Leitner, F. Chaumette, and P. Corke. Training deep neural networks for visual servoing. In *ICRA*, pages 1–8. IEEE, 2018.

[26] P. Florence, C. Lynch, A. Zeng, O. A. Ramirez, A. Wahid, L. Downs, A. Wong, J. Lee, I. Mordatch, and J. Tompson. Implicit behavioral cloning. In *CoRL*, pages 158–168. PMLR, 2022.

[27] A. I. Károly, P. Galambos, J. Kuti, and I. J. Rudas. Deep learning in robotics: Survey on model structures and training strategies. *IEEE Transactions on Systems, Man, and Cybernetics: Systems*, 51(1):266–279, 2020.

[28] Y. Labbe, J. Carpentier, M. Aubry, and J. Sivic. Cosypose: Consistent multi-view multi-object 6d pose estimation. In *ECCV*, 2020.

[29] I. Akkaya, M. Andrychowicz, M. Chociej, M. Litwin, B. McGrew, A. Petron, A. Paino, M. Plappert, G. Powell, R. Ribas, et al. Solving rubik's cube with a robot hand. *arXiv preprint arXiv:1910.07113*, 2019.

[30] R. Caruana. Learning many related tasks at the same time with backpropagation. *NeurIPS*, 7, 1994.

[31] H. B. Ammar, E. Eaton, P. Ruvolo, and M. Taylor. Online multi-task learning for policy gradient methods. In *ICML*, pages 1206–1214. PMLR, 2014.

[32] C. Devin, A. Gupta, T. Darrell, P. Abbeel, and S. Levine. Learning modular neural network policies for multi-task and multi-robot transfer. In *ICRA*, pages 2169–2176. IEEE, 2017.

[33] S. Sodhani, A. Zhang, and J. Pineau. Multi-task reinforcement learning with context-based representations. In *International Conference on Machine Learning*, pages 9767–9779. PMLR, 2021.

[34] T. Standley, A. Zamir, D. Chen, L. Guibas, J. Malik, and S. Savarese. Which tasks should be learned together in multi-task learning? In *International Conference on Machine Learning*, pages 9120–9132. PMLR, 2020.

[35] S. Thrun and J. O'Sullivan. Discovering structure in multiple learning tasks: The TC algorithm. In *ICML*, volume 96, pages 489–497, 1996.

[36] B. Chen, A. Sax, G. Lewis, I. Armeni, S. Savarese, A. Zamir, J. Malik, and L. Pinto. Robust policies via mid-level visual representations: An experimental study in manipulation and navigation. *CoRL*, 2020.

[37] C. Finn and S. Levine. Deep visual foresight for planning robot motion. In *ICRA*, pages 2786–2793. IEEE, 2017.

[38] T. Yu, C. Finn, A. Xie, S. Dasari, T. Zhang, P. Abbeel, and S. Levine. One-shot imitation from observing humans via domain-adaptive meta-learning. *RSS*, 2018.

[39] T. Yu, D. Quillen, Z. He, R. Julian, K. Hausman, C. Finn, and S. Levine. Meta-world: A benchmark and evaluation for multi-task and meta reinforcement learning. In *CoRL*, pages 1094–1100. PMLR, 2020.

[40] C. Finn, T. Yu, T. Zhang, P. Abbeel, and S. Levine. One-shot visual imitation learning via meta-learning. In *CoRL*, pages 357–368. PMLR, 2017.

[41] D. Kalashnikov, J. Varley, Y. Chebotar, B. Swanson, R. Jonschkowski, C. Finn, S. Levine, and K. Hausman. MT-Opt: Continuous multi-task robotic reinforcement learning at scale. *arXiv preprint arXiv:2104.08212*, 2021.

[42] A. S. Chen, S. Nair, and C. Finn. Learning generalizable robotic reward functions from "in-the-wild" human videos. *RSS*, 2021.

[43] R. S. Sutton and A. G. Barto. *Reinforcement learning: An introduction*. MIT press, 2018.

[44] T. Haarnoja, A. Zhou, K. Hartikainen, G. Tucker, S. Ha, J. Tan, V. Kumar, H. Zhu, A. Gupta, and P. Abbeel. Soft actor-critic algorithms and applications. *arXiv preprint arXiv:1812.05905*, 2018.

[45] J. Peters, S. Vijayakumar, and S. Schaal. Reinforcement learning for humanoid robotics. In *Proceedings of the third IEEE-RAS international conference on humanoid robots*, pages 1–20, 2003.

[46] A. Pashevich, D. Hafner, J. Davidson, R. Sukthankar, and C. Schmid. Modulated policy hierarchies. *NeurIPS Deep RL Workshop*, 2018.

[47] F. Torabi, G. Warnell, and P. Stone. Behavioral cloning from observation. In *Proceedings of the 27th International Joint Conference on Artificial Intelligence*, pages 4950–4957, 2018.

[48] J. Ho and S. Ermon. Generative adversarial imitation learning. *Advances in neural information processing systems*, 29, 2016.

[49] C. Lynch, M. Khansari, T. Xiao, V. Kumar, J. Tompson, S. Levine, and P. Sermanet. Learning latent plans from play. In *CoRL*, pages 1113–1132. PMLR, 2020.

[50] V. Petrík, M. Tapaswi, I. Laptev, and J. Sivic. Learning object manipulation skills via approximate state estimation from real videos. In *CoRL*, 2020.

[51] Y. Hristov, D. Angelov, M. Burke, A. Lascarides, and S. Ramamoorthy. Disentangled relational representations for explaining and learning from demonstration. In *CoRL*, 2019.

[52] G. Brockman, V. Cheung, L. Pettersson, J. Schneider, J. Schulman, J. Tang, and W. Zaremba. OpenAI Gym. *arXiv preprint arXiv:1606.01540*, 2016.

[53] K. Ehsani, W. Han, A. Herrasti, E. VanderBilt, L. Weihs, E. Kolve, A. Kembhavi, and R. Mottaghi. ManipulaTHOR: A framework for visual object manipulation. In *CVPR*, pages 4497–4506, 2021.

[54] S. Tunyasuvunakool, A. Muldal, Y. Doron, S. Liu, S. Bohez, J. Merel, T. Erez, T. Lillicrap, N. Heess, and Y. Tassa. dm_control: Software and tasks for continuous control. *Software Impacts*, 6:100022, 2020.

[55] F. Xiang, Y. Qin, K. Mo, Y. Xia, H. Zhu, F. Liu, M. Liu, H. Jiang, Y. Yuan, H. Wang, et al. Sapien: A simulated part-based interactive environment. In *Proceedings of the IEEE/CVF Conference on Computer Vision and Pattern Recognition*, pages 11097–11107, 2020.

[56] O. Ahmed, F. Träuble, A. Goyal, A. Neitz, Y. Bengio, B. Schölkopf, M. Wüthrich, and S. Bauer. CausalWorld: A robotic manipulation benchmark for causal structure and transfer learning. *arXiv preprint arXiv:2010.04296*, 2020.

[57] D. Misra, J. Langford, and Y. Artzi. Mapping instructions and visual observations to actions with reinforcement learning. *ACL*, 2017.

[58] E. Stengel-Eskin, A. Hundt, Z. He, A. Murali, N. Gopalan, M. Gombolay, and G. Hager. Guiding multi-step rearrangement tasks with natural language instructions. In *Conference on Robot Learning*, pages 1486–1501. PMLR, 2021.

[59] K. M. Hermann, F. Hill, S. Green, F. Wang, R. Faulkner, H. Soyer, D. Szepesvari, W. M. Czarnecki, M. Jaderberg, D. Teplyashin, M. Wainwright, C. Apps, D. Hassabis, and P. Blunso. Grounded language learning in a simulated 3D world. *NeurIPS Workshop*, 2017.

[60] D. I. A. Team, J. Abramson, A. Ahuja, A. Brussee, F. Carnevale, M. Cassin, F. Fischer, P. Georgiev, A. Goldin, T. Harley, et al. Creating multimodal interactive agents with imitation and self-supervised learning. *arXiv preprint arXiv:2112.03763*, 2021.

[61] R. Paul, J. Arkin, N. Roy, and T. M Howard. Efficient grounding of abstract spatial concepts for natural language interaction with robot manipulators. In *Robotics: Science and Systems Foundation*, 2016.

[62] T. Nguyen, N. Gopalan, R. Patel, M. Corsaro, E. Pavlick, and S. Tellex. Robot object retrieval with contextual natural language queries. *RSS*, 2020.

[63] W. Goodwin, S. Vaze, I. Havoutis, and I. Posner. Semantically grounded object matching for robust robotic scene rearrangement. *ICRA*, 2021.

[64] S. Tellex, T. Kollar, S. Dickerson, M. R. Walter, A. G. Banerjee, S. Teller, and N. Roy. Understanding natural language commands for robotic navigation and mobile manipulation. In *Twenty-Fifth AAAI Conference on Artificial Intelligence*, 2011.

[65] W. Liu, C. Paxton, T. Hermans, and D. Fox. StructFormer: Learning spatial structure for language-guided semantic rearrangement of novel objects. *ICRA*, 2021.

[66] W. Huang, P. Abbeel, D. Pathak, and I. Mordatch. Language models as zero-shot planners: Extracting actionable knowledge for embodied agents. *arXiv preprint arXiv:2201.07207*, 2022.

[67] D. Garg, S. Vaidyanath, K. Kim, J. Song, and S. Ermon. LISA: Learning interpretable skill abstractions from language. *arXiv preprint arXiv:2203.00054*, 2022.

[68] A. Khandelwal, L. Weihs, R. Mottaghi, and A. Kembhavi. Simple but effective: Clip embeddings for embodied ai. In *Proceedings of the IEEE/CVF Conference on Computer Vision and Pattern Recognition*, pages 14829–14838, 2022.

[69] A. Vaswani, N. Shazeer, N. Parmar, J. Uszkoreit, L. Jones, A. N. Gomez, Ł. Kaiser, and I. Polosukhin. Attention is all you need. *Advances in neural information processing systems*, 30, 2017.

[70] A. Dosovitskiy, L. Beyer, A. Kolesnikov, D. Weissenborn, X. Zhai, T. Unterthiner, M. Dehghani, M. Minderer, G. Heigold, S. Gelly, et al. An image is worth 16x16 words: Transformers for image recognition at scale. *ICLR*, 2020.

[71] H. Tan and M. Bansal. Lxmert: Learning cross-modality encoder representations from transformers. In *EMNLP*, 2019.

[72] L. Chen, K. Lu, A. Rajeswaran, K. Lee, A. Grover, M. Laskin, P. Abbeel, A. Srinivas, and I. Mordatch. Decision transformer: Reinforcement learning via sequence modeling. In *NeurIPS*, 2021.

[73] A. L. Putterman, K. Lu, I. Mordatch, and P. Abbeel. Pretraining for language conditioned imitation with transformers. In *NeurIPS*, 2021.

[74] S. Chen, P.-L. Guhur, C. Schmid, and I. Laptev. History aware multimodal transformer for vision-and-language navigation. *Advances in Neural Information Processing Systems*, 34, 2021.

[75] A. Pashevich, C. Schmid, and C. Sun. Episodic transformer for vision-and-language navigation. In *Proceedings of the IEEE/CVF International Conference on Computer Vision*, pages 15942–15952, 2021.

[76] P.-L. Guhur, M. Tapaswi, S. Chen, I. Laptev, and C. Schmid. Airbert: In-domain pretraining for vision-and-language navigation. In *Proceedings of the IEEE/CVF International Conference on Computer Vision*, pages 1634–1643, 2021.

[77] S. Reed, K. Zolna, E. Parisotto, S. G. Colmenarejo, A. Novikov, G. Barth-Maron, M. Gimenez, Y. Sulsky, J. Kay, J. T. Springenberg, et al. A generalist agent. *arXiv preprint arXiv:2205.06175*, 2022.

[78] J. L. Ba, J. R. Kiros, and G. E. Hinton. Layer normalization. *arXiv preprint arXiv:1607.06450*, 2016.

[79] A. Vaswani, N. Shazeer, N. Parmar, J. Uszkoreit, L. Jones, A. N. Gomez, L. Kaiser, and I. Polosukhin. Attention is all you need. *NeurIPS*, 2017.

[80] S. Ross, G. Gordon, and D. Bagnell. A reduction of imitation learning and structured prediction to no-regret online learning. In *Proceedings of the fourteenth international conference on artificial intelligence and statistics*, pages 627–635. JMLR Workshop and Conference Proceedings, 2011.

[81] S. James and P. Abbeel. Coarse-to-fine Q-Attention with learned path ranking. *arXiv preprint arXiv:2204.01571*, 2022.

[82] A. Silva, N. Moorman, W. Silva, Z. Zaidi, N. Gopalan, and M. Gombolay. Lancon-learn: Learning with language to enable generalization in multi-task manipulation. *IEEE Robotics and Automation Letters*, 7(2):1635–1642, 2021.

[83] E. Olson. Apriltag: A robust and flexible visual fiducial system. In *ICRA*, 2011.

Appendix

In this appendix we first present details about the model architecture in Section A. Then we describe our categorization for RLBench tasks in Section B and experimental details in Section C. We further provide additional ablations in Section D. Finally, we conduct real robot experiments in Section E and present both quantitative and qualitative results on the real robot.

A   Model Architecture

UNet encoder for image encoding. The CNN in Eq (2) of the main paper is composed of 6 convolutional layers. The first two layers use kernels of size 3x3, strides of size 1 and output channels of sizes 8 and 16 respectively with LeakyReLU activation function. The remaining four layers use 3x3 kernels, strides of size 2 and output channels of size 16 followed by group normalization and LeakyReLU activation function. Therefore, an image of size $H \times W \times 3$ is encoded by a feature map of size $\frac{H}{16} \times \frac{W}{16} \times 16$.

UNet decoder for position prediction. The decoder uses a sequence of convolutional and upsampling layers to generate a heatmap on the point clouds. Specifically, the convolutional layer is fed with the output from the previous layer and the residual connection from corresponding layer in the UNet encoder. Its output channel size is 16, kernel size is 3 and stride size is 1. The upsampling layer uses scale factor of 2 and bilinear sampling. We stack 4 blocks of the layers to recover the original image size $H \times W$.
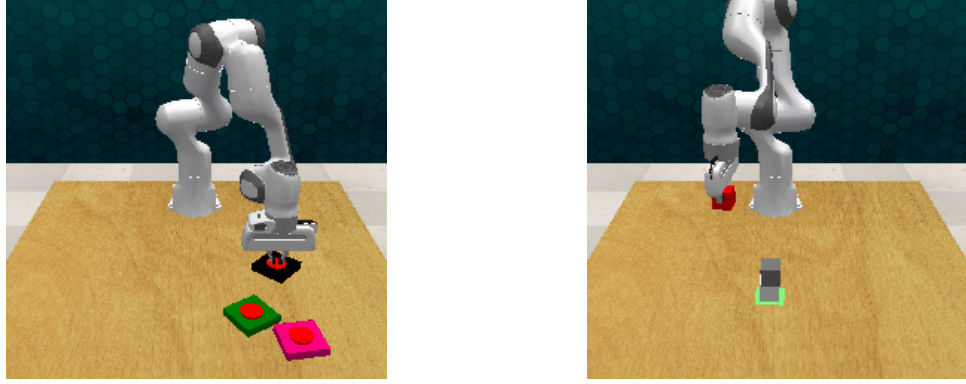
CNN for rotation and gripper. The CNN is composed of two convolutional layers, each with a 3x3 kernel, a stride of 2 and an output channel of size 64 followed by the group normalization and a LeakyReLU activation function. Then we apply average pooling and feed the flattened vector into a feedforward network to regress a 5-dimensional vector composed of 4-dimensional quaternion q_{t+1} and 1-dimensional gripper state c_{t+1}.

B   Categorization of RLBench Tasks

We evaluate on 74 available RLBench tasks. Although RLBench[2] currently contains 106 supported tasks, we had difficulties to produce demonstrations for 32 of them due to issues with the scripts and the motion planner. To analyze the performance of our model applied to different types of tasks, we manually group 74 tasks into 9 categories according to their key challenges. The 9 task groups are defined as follows:

- The **Planning** group contains tasks with multiple sub-goals (*e.g.* picking a basket ball and then throwing the ball). The included tasks are: basketball in hoop, put rubbish in bin, meat off grill, meat on grill, change channel, tv on, tower3, push buttons, stack wine.
- The **Tools** group is a special case of planning where a robot must grasp an object to interact with the target object. The included tasks are: slide block to target, reach and drag, take frame off hanger, water plants, hang frame on hanger, scoop with spatula, place hanger on rack, move hanger, sweep to dustpan, take plate off colored dish rack, screw nail.
- The **Long term** group requires more than 10 macro-steps to be completed. The included tasks are: wipe desk, stack blocks, take shoes out of box, slide cabinet open and place cups.
- The **Rotation-invariant** group can be solved without changes in the gripper rotation. The included tasks are: reach target, push button, lamp on, lamp off, push buttons, pick and lift, take lid off saucepan.
- The **Motion planner** group requires precise grasping. As observed in [81] such tasks often fail due to the motion planner. The included tasks are: toilet seat down, close laptop lid, open box, open drawer, close drawer, close box, phone on base, toilet seat up, put books on bookshelf.
- The **Multimodal** group can have multiple possible trajectories to solve a task due to a large affordance area of the target object (*e.g.* the edge of a cup). The included tasks are: pick up cup, turn tap, lift numbered block, beat the buzz, stack cups.
- The **Precision** group involves precise object manipulation. The included tasks are: take usb out of computer, play jenga, insert onto square peg, take umbrella out of umbrella stand, insert

---

[2]https://github.com/stepjam/RLBench/tree/master/rlbench/tasks

Figure 3: The tasks used in multi-variation setting. Left: push buttons task. Right: tower task.

usb in computer, straighten rope, pick and lift small, put knife on chopping board, place shape in shape sorter, take toilet roll off stand, put umbrella in umbrella stand, setup checkers.
- The **Screw** group requires screwing an object. The included tasks are: turn oven on, change clock, open window, open wine bottle.
- The **Visual Occlusion** group involves tasks with large objects and thus there are occlusions from certain views. The included tasks are: close microwave, close fridge, close grill, open grill, unplug charger, press switch, take money out safe, open microwave, put money in safe, open door, close door, open fridge, open oven, plug charger in power supply.

C Experimental Details

Motion Planner. We modified the default motion planner in RLBench, as it sometimes fails to reach a target pose even though there exist successful trajectories in the 3D space. To reduce the impact of the imperfect motion planner, we run the motion planner with different seeds up to 10 times until it finds a trajectory to the target.

Task Setup in Multi-variation Setting. For the multi-variation setting we choose tasks with as many variations as possible. We hence select the push buttons and tower tasks, for which we can easily construct new variations, as illustrated in Figure 3. For each of these tasks we use 100 variations for training and 100 different variations for testing.
- The **Push Buttons** task has three buttons with unique colors in the scene. The robot should press some or all of the buttons according to the order in an instruction. Variations of the task are defined by the different order and different colors of buttons. RLBench provides three sentence templates to generate synthetic instructions with changing button colors such as "push the red button, and then push the cyan one".
- The **Tower** task is inspired by the "stack block" task. The robot must stack some of the three colored cubes at a target location following the color order provided by the instruction. We generate synthetic instructions for each variation, such as "Stack the red, blue, green blocks", or "Stack the yellow block. Stack the purple block on top of it, then add the cyan cube".

Collection of human-written instructions. In addition to synthetic instructions used for training, we collect human-written natural language instructions for testing. We collect 162 human-written instructions and measure the success rate for each instruction on 10 episodes with random object locations. 8 native English speakers participated in the dataset collection, leading to 63 instructions of 51 testing variations for the push buttons task, and 99 instructions for 99 testing variations for the tower task. Human-written instructions are more varied than the synthetic ones. They contain unseen verbs (e.g. "Tap on the green button, then the grey button and end up pressing the pink button"), unseen formulations (e.g. "Press the green, cyan and pink buttons in that order"), longer sentences (e.g. "Press the white button and then you go to green button and press it and finally press the black button") or unseen color references (e.g. "Press the darker blue button, then the gray one and finally the lighter blue button.").

15

Table 6: Comparison with LanCon-Learn [82] on 10 tasks.

	Hist.	Pick & Lift	Pick-Up Cup	Push Button	Put Knife	Put Money	Reach Target	Slide Block	Stack Wine	Take Money	Take Umbrella	Avg.
Single-task learning												
LanCon-Learn	-	20.2	25.2	96.2	57.8	91.4	99.6	60.2	57.0	58.4	73.0	63.9
LanCon-Learn	✓	64.8	56.8	96.4	59.4	90.6	98.7	63.4	56.6	67.8	74.8	72.9
Ours	✓	92.2	77.1	99.6	69.7	96.2	100.0	95.4	81.9	82.1	90.1	88.4
Multi-task learning												
LanCon-Learn	-	18.2	23.2	80.2	28.8	59.6	100.0	38.8	25.2	58.2	45.6	47.8
LanCon-Learn	✓	52.6	44.2	81.5	32.2	75.6	100.0	42.2	24.6	70.2	50.8	57.4
Ours	✓	88.9	92.9	100.0	75.3	58.2	100.0	78.7	71.2	79.1	89.2	83.3

Table 7: Comparison with LanCon-Learn [82] and ablation of the instruction encoding in the multi-variation setting for seen or unseen variations and synthetic, corrupted or real instructions.

Method	Hist.	Instructions		Emb. E_T^x	Visual Emb. E_T^v	Push buttons				Tower			
		Format	Encoder			Seen	Unseen			Seen	Unseen		
						Synt.	Synt.	Corr.	Real	Synt.	Synt.	Corr.	Real
LanCon-Learn	No	Cat.	GloVe	-	-	25.6	12.1	0.3	0.1	21.3	9.1	0.1	0.0
LanCon-Learn	Yes	Cat.	GloVe	-	-	37.8	16.7	1.6	0.9	34.9	14.2	1.2	0.8
Ours	No	Seq.	CLIP	✓	✓	8.6	3.6	0.3	0.1	7.1	4.5	0.2	0.0
Ours	Yes	Avg.	CLIP	✓	✓	9.1	1.1	0.0	0.0	5.3	0.2	0.0	0.0
Ours	Yes	Seq.	CLIP	-	✓	100	83.2	81.1	71.3	77.1	53.2	51.3	21.3
Ours	Yes	Seq.	CLIP	-	-	86.2	65.2	56.4	49.8	54.9	34.8	29.8	24.7
Ours	Yes	Seq.	BERT	✓	✓	54.6	40.2	15.6	21.8	42.9	28.9	8.2	10.2
Ours	Yes	Seq.	OHE	✓	✓	100	3.1	0.1	0.0	96.8	3.8	0.4	0.0
Ours	Yes	Seq.	CLIP	✓	✓	100	86.3	85.6	74.2	77.4	56.2	53.6	24.1

D Experiments on the simulator RLBench

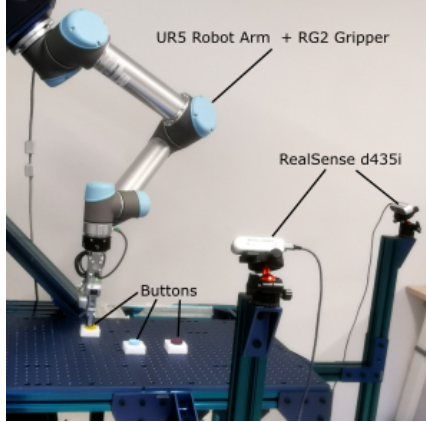We conducted further ablation studies to confirm our approach.

D.1 Comparison with Additional State-of-the-Art Approach

LanCon-Learn [82] is a recent instruction-conditioned multi-task approach. It takes as input the gripper state and the object state, namely the ground truth pose of each object in the scene, instead of raw visual observations as ours. It encodes instructions with GloVe embeddings and a bi-directional LSTM. It predicts the next pose of the gripper based on a modular architecture conditioned on encoded text features. We run experiments on RLBench with the code provided by the authors. Since some RLBench tasks require identifying the colors of an object, we modify their object state to include a RGB reference of each object. Moreover, we complete their method with a history mechanism, where the gripper state is concatenated with the gripper state from the previous step.

As described in Table 6, we obtained an average success rate of 63.9% with their original method (vs. 72.9% with history vs. 88.3% for our approach) in our single-task setting and 47.8% (vs. 57.4% with history vs. 83.8% for our approach) in our multi-task setting.

D.2 Additional Ablations on Multi-variation Setting

In the multi-variation setting in Table 7, the gap between LanCon-Learn and our approach is more significant than in Table 6, since GloVe embeddings differentiate poorly colors: for the "push buttons" task on unseen variations and synthetic instructions, the performance reaches only 1.7% (vs. 86.3% with our approach). This also happens when replacing CLIP embeddings with BERT in our model (40.2%).

The important role of history for long-term planning tasks such as "pushing buttons" is confirmed when comparing LanCon-Learn or our model with and without history in the Table 7. The model without history can only use its current observation to predict the next action. Therefore, it is hard to infer which buttons have been pressed and which button is the next target, leading to poor performance on the task.

Figure 4: The robot scene with two RGB-D cameras and a UR5 robotics arm with an RG2 gripper.

We found that removing E_T^x decreases the performance only by 3.1%, but removing both E_T^x and E_T^y decreases the performance by 21.1%. Moreover, replacing the instructions with one-hot encoding of the variation index increases the performance for seen variations (by 19.4% on the tower task), but prevents the model from generalizing to unseen variations.

We performed ablations with corrupted instructions on unseen variations. Corrupted instructions were created from synthetic instructions by replacing color references with synonyms that have not been seen during training. For example, the color "azure" is replaced with "light blue", and the color "maroon" with "dark red". Baselines using CLIP as a language encoder have a much smaller drop of performance than any other encoder.

We also test our model with a global language embedding (average over word tokens) as in [9] and observe a significant drop in performance. The main reason is that the averaged embeddings do not represent well different action orders, *e.g.* we have obtained the average cosine similarity of 0.97 for instructions corresponding to same actions in different orders.
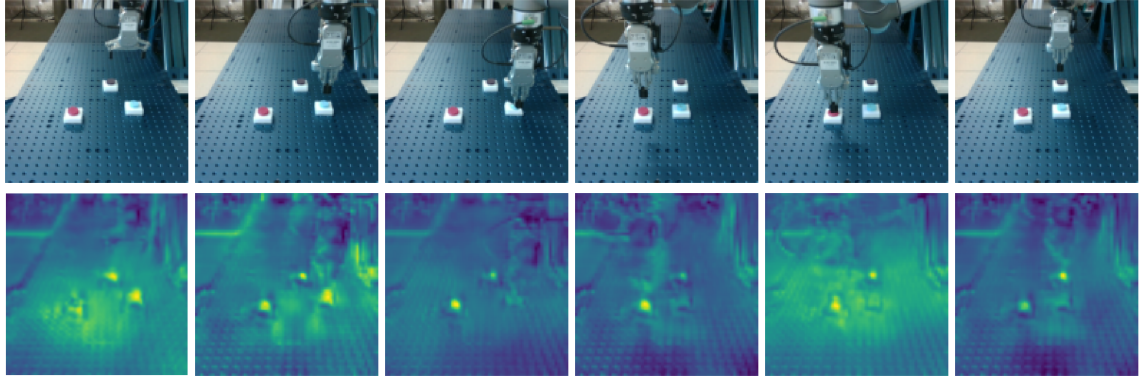
E   Experiments on Real-robot

Setup details. The cameras are Intel RealSense RGB-D cameras mounted on a fixed support as illustrated in Figure 4. We adapt our model to use $K = 2$ cameras. The resolution of the captured images is at a resolution of 1280×720, we apply center crop and downsampling to obtain images of size 128×128, which is the input to our model. We use nearest approximation to downsample depth images and bilinear approximation for RGB images. We use intrinsic parameters provided by Intel, and perform extrinsic calibration between the camera and the robot base-frame using an AprilTag marker [83]. We built 10 buttons using white cellulose foams: we manually cut them into 5×5 cm squares and attached to each square a painted rounded foam. The button bases and buttons have an average size of 4.95 ± 0.1 cm and 3.18 ± 0.22 cm respectively.

To collect demonstrations with the real robot, we design a script that automatically solves the task provided ground truth locations of buttons and the correct sequence of actions. In each demonstration objects are placed at random locations on the workspace and actions are executed at 10 Hz. We finetune the model for 8k iterations using the same training setup as that in the simulator.

Qualitative Results. Figure 5 shows a successful example from our real robot experiments. The attention maps reveal that the robot correctly attends to the next buttons. Thanks to the history of previous observations and actions, the model is confident to not press a button that has already been pressed before (for example the cyan in the fourth column).

In Figure 6, we analyze the robustness of our model for to unseen variations in more challenging situations. The instruction of the variation is written by human: *"Press the yellow button and then press the black button and finish with the white button"*. Our model successfully pressed the buttons in the correct order for all situations in Figure 6.

- Figure 6a: Since the foam buttons have low friction with the table, the gripper has accidentally flipped the black button, providing two buttons looking white. However, thanks to its

Figure 5: The instruction is "Press the cyan button, and then press the rose one, and then press the purple one". Top row: sequence of observations from one of the two side cameras in the robot scene. Bottom row: sequence of predicted attention maps by our model that indicate the gripper's position for the next step.

history component, the robot is able to successfully press the right white button instead of the flipped button.

- Figure 6b: Two white buttons are present in the scene. This is a multi-modal example, in which the robot might predict a mean position between the two white buttons, whereas our robot can cope with this challenge.

- Figure 6c: We use a ruler to move the location the white button in the scene after the robot pushed the yellow button. Although such perturbations have never been used in training sequences, the robot remains robust to this dynamic environment.

- Figure 6d: We change the shape of the button by increasing the height of the yellow button.

- Figure 6e: We add occlusion to the gripper.

- Figure 6f: We change the appearance of the table. Our model is robust to the above visual modifications.
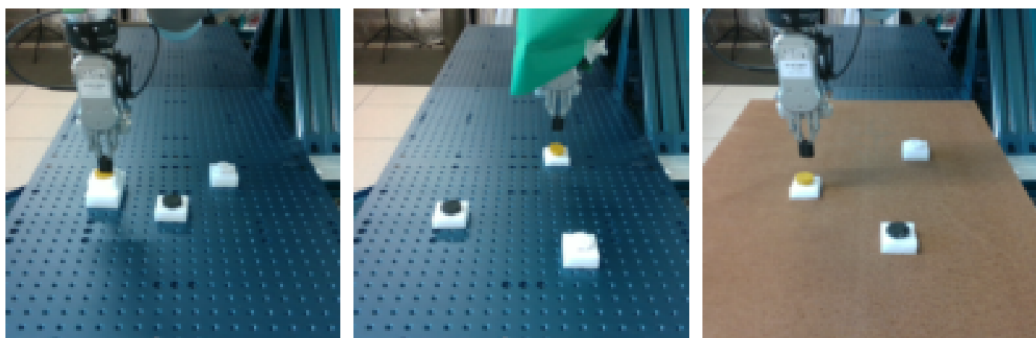
More details and video demonstrations of our real-robot experiments are available from the project webpage [1].

(a) Flipped button.   (b) Multimodal.   (c) Dynamic Environment.

(d) Unseen Button.   (e) Unseen Gripper.   (f) Unseen Table.

Figure 6: Robustness of the learned policy on an unseen variation: *"Press the yellow button and then press the black button and finish with the white button"*.